Geophysical Journal International

Geophys. J. Int. (2014) **197,** 1033–1047
Advance Access publication 2014 February 21

doi: 10.1093/gji/ggu032

Optimal staggered-grid finite-difference schemes based on least-squares for wave equation modelling

Yang Liu

State Key Laboratory of Petroleum Resources and Prospecting and CNPC Key Laboratory of Geophysical Prospecting, China University of Petroleum, Beijing, China. E-mail. wliuyang@vip.sina.com

Accepted 2014 January 27. Received 2014 January 21; in original form 2013 May 17

SUMMARY

I develop least-squares (LS)-based schemes to derive globally optimal spatial explicit staggered-grid finite-difference (SGFD) coefficients of the first-order derivative over a given wavenumber range for a given operator length, with no iterations involved. Dispersion analyses show that the dispersion error reduces with an increase of the operator length and a decrease of the wavenumber range. Therefore, globally optimal spatial SGFD coefficients with the shortest operator length can be found to satisfy the given error limitation in the given wavenumber range. Examples of optimal explicit SGFD coefficients are given. In addition, a LS-based scheme to derive optimal implicit SGFD coefficients is meanwhile put forward. Examples of optimal implicit SGFD coefficients are given. Numerical experiments for a homogeneous model and a heterogeneous model demonstrate that the LS-based SGFD method has a higher accuracy than the Taylor-series expansion (TE)-based SGFD method for the same operator length. Compared to the TE-based SGFD method, the LS-based SGFD method can adopt a shorter operator to achieve the same accuracy and thus is more efficient.

Key words: Numerical solutions; Computational seismology; Wave propagation.

1 INTRODUCTION

Compared with conventional standard-grid finite-difference (FD) methods, staggered-grid FD (SGFD) methods have been more widely used in numerically solving wave equations for their greater precision and stability, though some non-staggered schemes (e.g. Zhang & Chen 2006; Tarrass *et al.* 2011; Zhang *et al.* 2012) have been successfully developed to simulate seismic wave propagation. Madariaga (1976) developed a SGFD scheme for crack propagation modelling. Virieux (1984, 1986) advanced SGFD schemes for simulating *SH* and *P-SV* wave propagation in 2-D elastic media. These schemes are second-order accurate. Levander (1988) described a SGFD scheme with the fourth-order accuracy in space and the second-order accuracy in time for 2-D *P-SV* wave modelling. Graves (1996) presented a SGFD scheme to model wave propagation in 3-D elastic media. Moczo *et al.* (2000) studied the stability and the grid dispersion of 3-D fourth-order displacement-stress and velocity-stress SGFD schemes. Moczo *et al.* (2002) proposed a new 3-D fourth-order SGFD scheme for modelling seismic motion and seismic wave propagation. Some researchers (e.g. Zhang 1997; Gottschämer & Olsen 2001; Kristek *et al.* 2002; Mittet 2002; Lan & Zhang 2011) studied implementation of free surface boundary conditions involved in elastic SGFD modelling. Surface topography can also be included in SGFD modelling (e.g. Ohminato & Chouet 1997; Hestholm & Ruud 1998; Hestholm 2003; Lombard *et al.* 2008). In the past 20 yr, SGFD methods have been applied in visco-acoustic and viscoelastic wave modelling (e.g. Robertsson *et al.* 1994a; Robertsson 1996; Hayashi *et al.* 2001; Bohlen 2002; Operto *et al.* 2007).

To settle the instability of standard-grid FD modelling in high contrasts elastic media, Saenger *et al.* (2000) employed a partly staggered scheme, which has all stress/tensor components at the centre of a grid cell and all displacement/velocity components at each corner of the cell. Upon their demonstration, its advantages have been taken to simulate elastic waves propagation, especially in media containing cracks, pores or free surfaces (e.g. Saenger & Shapiro 2002; Krüger *et al.* 2005), anisotropic media (Saenger & Bohlen 2004; Bansal & Sen 2008) and viscoelastic media (Yan & Liu 2012).

High-order methods, including explicit methods (e.g. Crase 1990; Dong *et al.* 2000; Etgen & O'Brien 2007; Hestholm 2009; Di Bartolo *et al.* 2012) as well as implicit methods (e.g. Lele 1992; Liu & Sen 2009a; Du *et al.* 2009), etc., have been universally adopted to improve the accuracy of spatial SGFD. FD coefficients are usually determined by the Taylor-series expansion (TE; e.g. Fornberg 1987, 1988; Liu *et al.* 1998; Song & Fomel 2011; Chu & Stoffa 2012a). The TE-based method (TEM) uses TE to expand trigonometric functions in SGFD dispersion relations into polynomials, whose coefficients are applied to derive SGFD coefficients (e.g. Liu & Sen 2009a). The TEM usually provides a very high accuracy

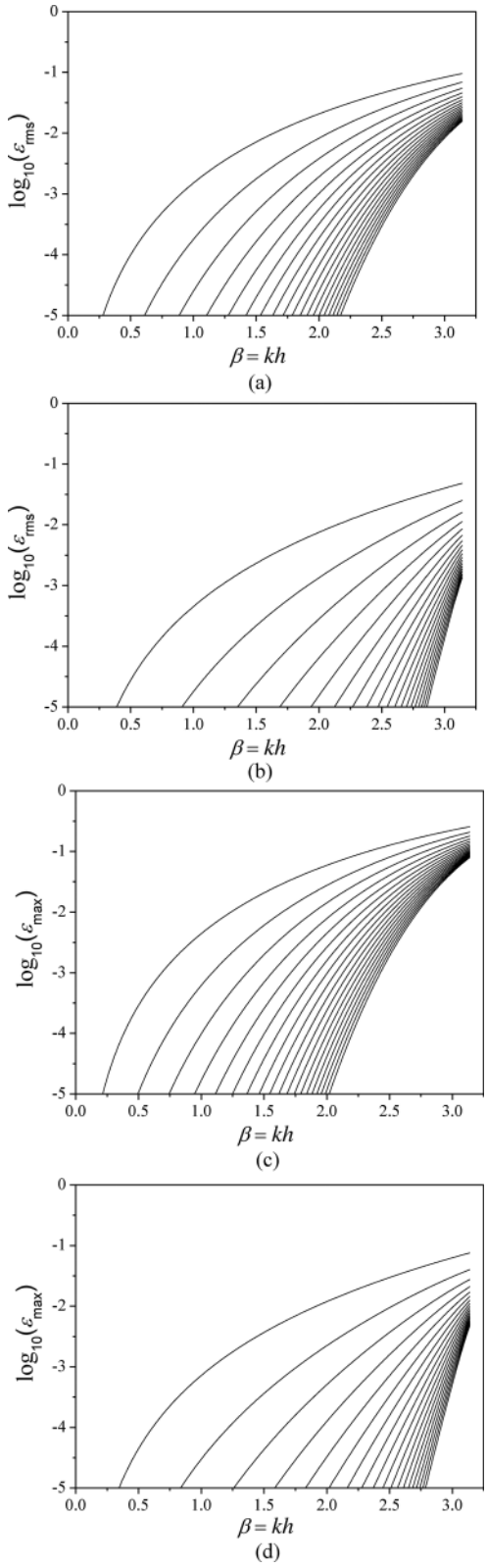

Figure 1. Variations of $\log_{10}(\varepsilon_{\rm rms})$ and $\log_{10}(\varepsilon_{\rm max})$ of ESGFD with b for different M by the TEM and the LSM of minimizing the absolute error of dispersion relation, respectively. Variations of $\log_{10}(\varepsilon_{\rm rms})$ with b are shown in (a) by the TEM and (b) by the LSM. Variations of $\log_{10}(\varepsilon_{\rm max})$ with b are shown in (c) by the TEM and (d) by the LSM. From top to bottom, lines are from $M = 2, 3, \ldots, 20$, respectively.

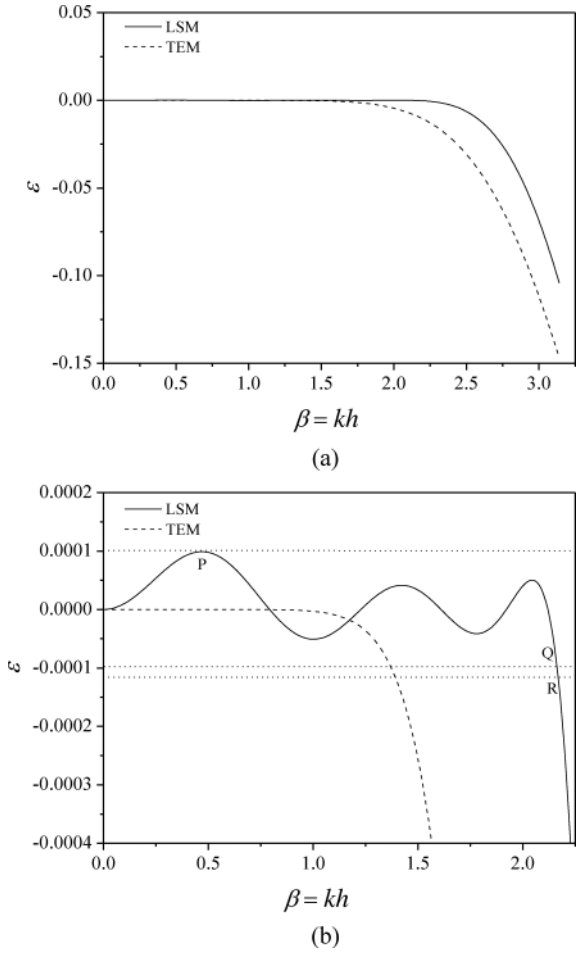

Figure 2. $\varepsilon(\beta)$ of ESGFD in (a) and its zoom in (b) by the TEM and the LSM of minimizing the absolute error of dispersion relation, respectively. $M = 6$. For the LSM, $b = 2.17$ is used in eq. (12) together with (11) and (9) to calculate c_m, and their values are shown in Table 3. At the points R and Q, $\beta = b$ and $\beta = B$. At the points P and Q, $|\varepsilon|$ have the same value.

over a small wavenumber range, but it has to adopt a long operator to obtain a high accuracy over a large wavenumber range and thus takes great computational time.

To obtain a high accuracy at a low computational cost, truncation-based methods (e.g. Zhou & Greenhalgh 1992; Igel *et al.* 1995; Liu & Sen 2009b) and optimization-based methods (e.g. Tam & Webb 1993; Takeuchi & Geller 2000; JafarGandomi & Takenaka 2009) have been developed to derive FD coefficients. The truncation-based methods obtain FD coefficients by truncating spatial convolution series of the pseudospectral method (e.g. Zhou & Greenhalgh 1992; Igel *et al.* 1995), omitting small values in the TE-based high-order FD coefficients (Liu & Sen 2009b; Chang & Liu 2013) or using scaled binomial windows (Chu & Stoffa 2012b) to reduce the operator length while maintaining the same approximate accuracy. The truncation-based methods are easy to use but do a little to improve the accuracy and reduce the computation cost.

Optimization-based methods are usually adopted to compute optimized FD coefficients at a given wavenumber range and operator length, commonly using gradient-like algorithms, such as the least-squares (LS) method, to minimize FD dispersion relations (e.g. Tam & Webb 1993; Yang & Balanis 2006; Shan 2009; Kosloff *et al.* 2010; Zhou & Zhang 2011; Liu 2013), phase velocity errors

Table 1. The B values of ESGFD for different M and maximum relative errors η from the TEM and the LSM of minimizing the absolute error of dispersion relation, respectively. $\varepsilon_{\max} < \eta$ is satisfied in the interval $[0, B]$.

M	B					
	$\eta = 10^{-3}$		$\eta = 10^{-4}$		$\eta = 10^{-5}$	
	TEM	LSM	TEM	LSM	TEM	LSM
2	0.68	1.04	0.38	0.59	0.21	0.32
3	1.08	1.73	0.73	1.19	0.49	0.81
4	1.36	2.13	1.00	1.63	0.74	1.24
5	1.56	2.38	1.21	1.94	0.94	1.57
6	1.71	2.53	1.37	2.16	1.11	1.82
7	1.83	2.64	1.50	2.31	1.24	2.00
8	1.92	2.72	1.61	2.43	1.36	2.15
9	2.00	2.79	1.70	2.52	1.46	2.26
10	2.07	2.84	1.77	2.59	1.54	2.36
11	2.12	2.87	1.84	2.65	1.61	2.43
12	2.17	2.90	1.90	2.69	1.68	2.50
13	2.22	2.93	1.95	2.73	1.74	2.55
14	2.26	2.95	2.00	2.77	1.79	2.60
15	2.29	2.97	2.04	2.80	1.83	2.64
16	2.32	2.98	2.08	2.82	1.88	2.67
17	2.35	2.99	2.11	2.84	1.92	2.71
18	2.38	3.00	2.14	2.86	1.95	2.74
19	2.40	3.01	2.17	2.88	1.98	2.76
20	2.42	3.02	2.20	2.89	2.01	2.78
30	2.57	3.07	2.39	2.99	2.23	2.91
40	2.66	3.10	2.50	3.03	2.36	2.98
50	2.72	3.11	2.57	3.05	2.45	3.01

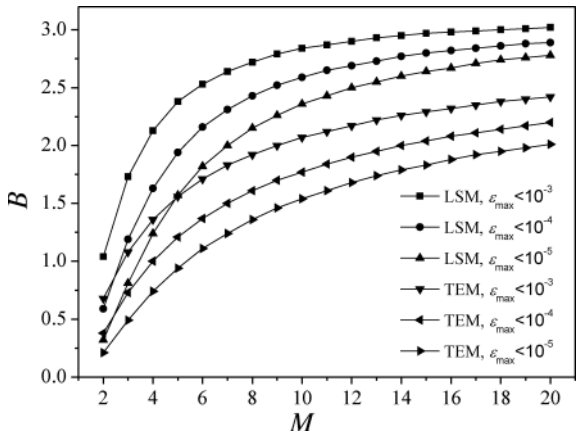

Figure 3. Variations of B of ESGFD with M for different maximum errors η by the TEM and the LSM of minimizing the absolute error of dispersion relation, respectively. $\varepsilon_{\max} < \eta$ in the interval $[0, B]$.

(e.g. Chen 2012) or group velocity errors (e.g. Jastram & Behle 1993; Robertsson *et al.* 1994b) over a wavenumber range (e.g. Jastram & Behle 1993; Tam & Webb 1993; Yang & Balanis 2006; Zhou & Zhang 2011; Chen 2012) or a frequency range (e.g. Robertsson *et al.* 1994b; Shan 2009). To maximize the wavenumber range at a given accuracy and operator length, Holberg (1987) designed FD coefficients by minimizing the peak relative error of group velocity. Kindelan *et al.* (1990) put forward an alternative frame to simplify the computation of Holberg's operators and used Newton's method to solve the optimization problem. Because gradient-like algorithms are locally optimal and may not obtain the global optimum, Zhang & Yao (2012, 2013) tried to obtain the best optimized FD coefficients and the bandwidth through simulated annealing of

Table 2. The b values of ESGFD used to calculate LS-based ESGFD coefficients by minimizing the absolute error of dispersion relation for different M and maximum relative errors η. $\varepsilon_{\max} < \eta$ is satisfied in the interval $[0, B]$, B is shown in Table 1.

M	b		
	$\eta = 10^{-3}$	$\eta = 10^{-4}$	$\eta = 10^{-5}$
2	1.08	0.61	0.34
3	1.76	1.21	0.83
4	2.16	1.65	1.25
5	2.40	1.95	1.58
6	2.55	2.17	1.83
7	2.66	2.32	2.01
8	2.74	2.44	2.16
9	2.80	2.53	2.27
10	2.85	2.60	2.37
11	2.88	2.66	2.44
12	2.91	2.70	2.51
13	2.94	2.74	2.56
14	2.96	2.78	2.60
15	2.98	2.81	2.64
16	2.99	2.83	2.68
17	3.00	2.85	2.71
18	3.01	2.87	2.74
19	3.02	2.89	2.76
20	3.03	2.90	2.78
30	3.08	3.00	2.91
40	3.11	3.04	2.98
50	3.12	3.06	3.01

global optimization algorithms. The current global optimization-based methods, with the highest computational expense, may not find the best optimization solution.

Liu (2013) proposed a LS-based scheme to derive globally optimal FD coefficients for second-order spatial derivatives, computing them over a given wavenumber range using the LS method, with no iterations involved. The results showed that the FD accuracy tends to increase as the operator length increases and the wavenumber range drops. Therefore, for a given error and operator length, globally optimal spatial FD coefficients can be obtained. This paper develops optimal explicit SGFD (ESGFD) and implicit SGFD (ISGFD) schemes based on the LS method. Dispersion analyses and numerical modelling demonstrate that the optimal ESGFD and ISGFD methods can significantly improve the modelling accuracy or reduce the computational cost compared to the TE-based ESGFD and ISGFD methods.

2 OPTIMAL ESGFD SCHEMES

2.1 ESGFD coefficients calculated with the LS method

An ESGFD operator involving $2M$ points is used to calculate the first-order derivative of a function $p(x)$ (Kindelan *et al.* 1990; Liu & Sen 2009a), that is,

$$\frac{\partial p}{\partial x} \approx \frac{1}{h}\sum_{m=1}^{M} c_m \left[p(x + mh - 0.5h) - p(x - mh + 0.5h)\right], \qquad (1)$$

where x is a real variable, h is a small positive value and c_m are FD coefficients.

Let

$$p(x + mh) = p_0 \exp\left[\mathrm{i}k(x + mh)\right], \qquad (2)$$

Table 3. Optimized ESGFD coefficients by the LSM of minimizing the absolute error of dispersion relation for the maximum relative error $\eta = 10^{-4}$.

Coefficient	$M=2$	$M=3$	$M=4$	$M=5$	
c_1	0.1129136E+1	0.1186247E+1	0.1218159E+1	0.1236425E+1	
c_2	−0.4304542E-1	−0.7266808E-1	−0.9397218E-1	−0.1081130E+0	
c_3		0.6351497E-2	0.1519043E-1	0.2339911E-1	
c_4			−0.1742128E-2	−0.5061550E-2	
c_5				0.7054313E-3	
Coefficient	$M=6$	$M=7$	$M=8$	$M=9$	$M=10$
c_1	0.1247576E+1	0.1254380E+1	0.1259012E+1	0.1262147E+1	0.1264362E+1
c_2	−0.1174969E+0	−0.1235307E+0	−0.1277647E+0	−0.1306967E+0	−0.1327958E+0
c_3	0.2997288E-1	0.3467231E-1	0.3820715E-1	0.4075792E-1	0.4264687E-1
c_4	−0.8741572E-2	−0.1192915E-1	−0.1458251E-1	−0.1665221E-1	−0.1824918E-1
c_5	0.2262285E-2	0.4057090E-2	0.5845385E-2	0.7377057E-2	0.8656223E-2
c_6	−0.3745306E-3	−0.1191005E-2	−0.2213861E-2	−0.3258150E-2	−0.4200034E-2
c_7		0.2263204E-3	0.7243880E-3	0.1336259E-2	0.1989180E-2
c_8			−0.1566173E-3	−0.4775830E-3	−0.8686637E-3
c_9				0.1151664E-3	0.3342741E-3
c_{10}					−0.8854090E-4

where p_0 is a constant value, $\mathrm{i} = \sqrt{-1}$, k represents the wavenumber. Substitute eq. (2) into (1) and obtain

$$2\sum_{m=1}^{M} c_m \sin\left[(m-0.5)\beta\right] \approx \beta, \tag{3}$$

where $\beta = kh$, and it only ranges from 0 to π because kh equals π at the Nyquist frequency.
Let

$$\varphi_m(\beta) = 2\sin\left[(m-0.5)\beta\right], \quad f(\beta) = \beta. \tag{4}$$

Then

$$\sum_{m=1}^{M} c_m \varphi_m(\beta) \approx f(\beta). \tag{5}$$

When the TE-based strategy is employed to calculate ESGFD coefficients, (2M)th-order accuracy can be obtained. Generally, the TE-based ESGFD coefficients can be used to compute accurate derivatives within the interval $[0, b]$ of β. Outside this interval, the accuracy of calculated derivatives tends to drop as β increases (Liu & Sen 2009a).

Optimal ESGFD coefficients can be calculated by minimizing the square error over a given interval $[0, b]$ $(0 < b < \pi)$ as follows:

$$E = \int_0^b \left[\sum_{m=1}^{M} c_m \varphi_m(\beta) - f(\beta)\right]^2 \mathrm{d}\beta. \tag{6}$$

Because $\varphi_1(\beta), \varphi_2(\beta), \ldots, \varphi_M(\beta)$ are linearly independent on the interval $[0, b]$, globally optimal c_m can be obtained by solving the following equations using the LS method,

$$\sum_{m=1}^{M}\left[\int_0^b \varphi_m(\beta)\varphi_n(\beta)d\beta\right] c_m = \int_0^b f(\beta)\varphi_n(\beta)d\beta, \ (n = 1, 2, \ldots, M). \tag{7}$$

Constraint conditions are usually adopted to improve the accuracy of optimal FD stencils near zero wavenumber (e.g. Zhou & Zhang 2011; Zhang & Yao 2013; Liu 2013). I introduce the following constraint condition:

$$2\sum_{m=1}^{M} c_m \sin\left[(m-0.5)\beta\right] \to \beta \text{ while } \beta \to 0. \tag{8}$$

Then, I obtain

$$c_1 = 1 - \sum_{m=2}^{M} (2m-1)c_m. \tag{9}$$

Substituting eq. (9) into (6) and using (4), I obtain

$$E = \int_0^b \left[\sum_{m=2}^{M} c_m \psi_m(\beta) - g(\beta)\right]^2 \mathrm{d}\beta, \tag{10}$$

where

$$\psi_m(\beta) = 2\left\{\sin\left[(m-0.5)\beta\right] - 2(m-0.5)\sin(0.5\beta)\right\},$$
$$g(\beta) = \beta - 2\sin(0.5\beta). \tag{11}$$

It should be noted that $\psi_2(\beta), \psi_3(\beta), \ldots, \psi_M(\beta)$ are still linearly independent on the interval $[0, b]$. With the LS method, globally optimal c_m $(m = 2, 3, \ldots, M)$ can be obtained by solving

$$\sum_{m=2}^{M}\left[\int_0^b \psi_m(\beta)\psi_n(\beta)\mathrm{d}\beta\right] c_m = \int_0^b g(\beta)\psi_n(\beta)\mathrm{d}\beta, \ (n = 2, 3, \ldots, M). \tag{12}$$

c_1 can be obtained by using eq. (9).

Usually, the ESGFD error is expected to be small in the given interval $[0, b]$ $(b > 0)$. The expected error for any given interval decreases as the ESGFD operator length increases. Therefore, it is possible to find the shortest length of the ESGFD operator for the given interval and the expected error.

2.2 Accuracy analysis

I compare the ESGFD accuracy of the TEM with that of the LS-based method (LSM). TE-based ESGFD coefficients for first-order derivatives can be obtained from the following formulae

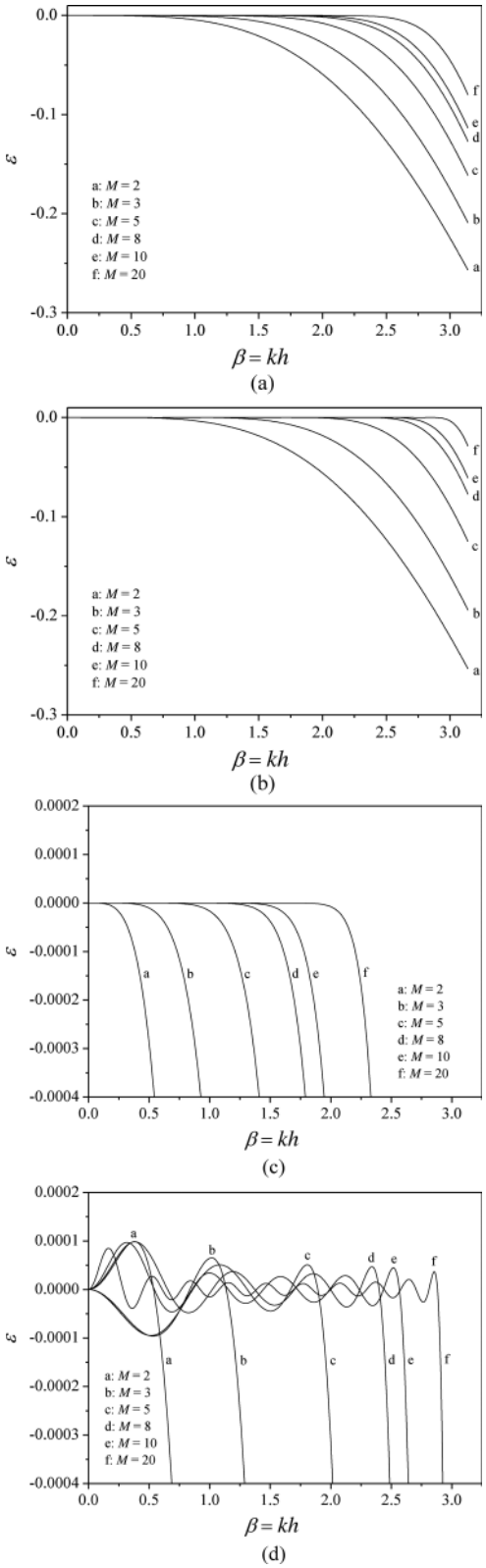

Figure 4. $\varepsilon(\beta)$ of ESGFD for different M by the TEM and the LSM of minimizing the absolute error of dispersion relation, respectively. (a) is by the TEM and (b) by the LSM. (c) is zoom of (a) and (d) is zoom of (b). FD coefficients of the LSM with the maximum error $\eta = 10^{-4}$ used in the figure ($M = 2, 3, 5, 8, 10$) are listed in Table 3.

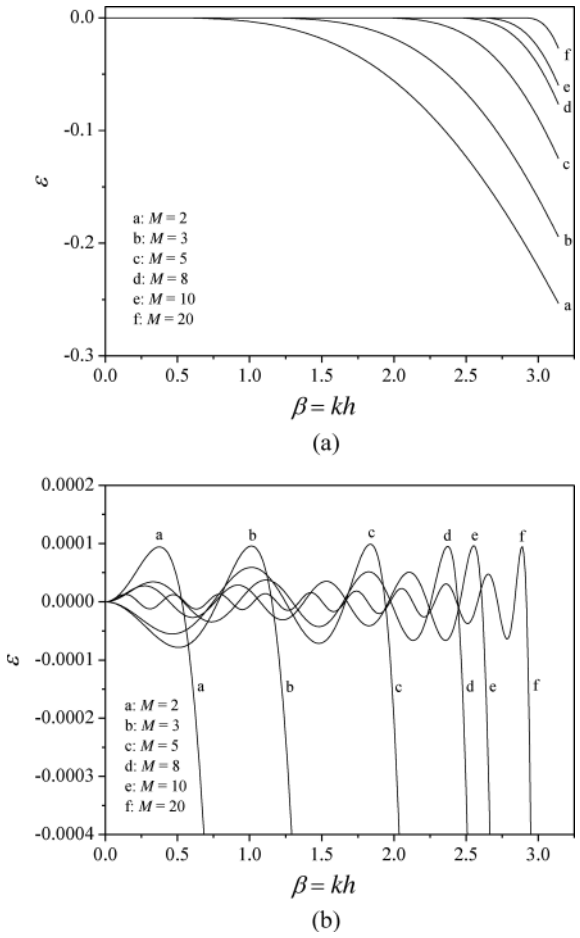

Figure 5. $\varepsilon(\beta)$ of ESGFD for different M by the LSM of minimizing the relative error of dispersion relation. (b) is zoom of (a). FD coefficients of the LSM with the maximum error $\eta = 10^{-4}$ used in the figure ($M = 2, 3, 5, 8, 10$) are listed in Table 6.

(e.g. Liu & Sen 2009a; Pei *et al.* 2012):

$$c_m = \frac{(-1)^{m+1}}{2m-1} \prod_{1 \le n \le M, n \ne m} \left| \frac{(2n-1)^2}{(2m-1)^2 - (2n-1)^2} \right|,$$

$$(m = 1, 2, \ldots, M). \tag{13}$$

To examine the accuracy, I calculate the variation of the rms error ε_r and the maximum error ε_{max} with b and M using

$$\varepsilon_{rms} = \sqrt{\frac{1}{b} \int_0^b \varepsilon^2(\beta) d\beta}, \tag{14}$$

$$\varepsilon_{max} = \max_{\beta \in [0,b]} |\varepsilon(\beta)|, \tag{15}$$

where

$$\varepsilon(\beta) = 2\beta^{-1} \sum_{m=1}^{M} c_m \sin[(m - 0.5)\beta] - 1. \tag{16}$$

Fig. 1 shows variations of $\log_{10}(\varepsilon_{rms})$ and $\log_{10}(\varepsilon_{max})$ with b for different M by the TEM and the LSM, respectively. From top to bottom of the figure, lines represent $M = 2, 3, \ldots, 20$, respectively. This figure suggests that

(1) When M is fixed, the error increases with an increase of b.
(2) When b is fixed, the error decreases with an increase of M.

Table 4. The B values of ESGFD for different M and maximum relative errors η from the TEM and the LSM of minimizing the relative error of dispersion relation, respectively. $\varepsilon_{\max} < \eta$ is satisfied in the interval $[0, B]$.

M	B		
	$\eta = 10^{-3}$	$\eta = 10^{-4}$	$\eta = 10^{-5}$
2	1.04	0.58	0.32
3	1.74	1.20	0.82
4	2.15	1.65	1.26
5	2.40	1.97	1.59
6	2.57	2.18	1.84
7	2.67	2.35	2.03
8	2.76	2.46	2.19
9	2.81	2.55	2.30
10	2.86	2.62	2.39
11	2.90	2.68	2.47
12	2.93	2.73	2.53
13	2.95	2.77	2.58
14	2.97	2.80	2.63
15	2.98	2.83	2.67
16	3.00	2.85	2.70
17	3.01	2.87	2.74
18	3.03	2.89	2.77
19	3.03	2.90	2.79
20	3.04	2.92	2.81
30	3.08	3.01	2.93
40	3.10	3.05	2.99
50	3.12	3.07	3.02

Table 5. The b values of ESGFD used to calculate LS-based ESGFD coefficients by minimizing the relative error of dispersion relation for different M and maximum relative errors η. $\varepsilon_{\max} < \eta$ is satisfied in the interval $[0, B]$, B is shown in Table 4.

M	b		
	$\eta = 10^{-3}$	$\eta = 10^{-4}$	$\eta = 10^{-5}$
2	1.13	0.63	0.35
3	1.82	1.25	0.86
4	2.22	1.70	1.29
5	2.46	2.01	1.62
6	2.62	2.22	1.87
7	2.72	2.38	2.06
8	2.80	2.49	2.21
9	2.85	2.58	2.32
10	2.90	2.65	2.41
11	2.93	2.70	2.49
12	2.96	2.75	2.55
13	2.98	2.79	2.60
14	3.00	2.82	2.65
15	3.01	2.85	2.69
16	3.03	2.87	2.72
17	3.04	2.89	2.75
18	3.05	2.91	2.78
19	3.05	2.92	2.80
20	3.06	2.94	2.82
30	3.10	3.02	2.94
40	3.12	3.06	3.00
50	3.13	3.08	3.03

(3) For the same error, the LSM has a wider wavenumber range than the TEM.

Therefore, one can find the unique b for any given M which provides the chosen maximum error η. Thus, ESGFD coefficients can be obtained using eq. (12) together with (11). This solution is globally optimal.

2.3 A globally optimal ESGFD scheme based on minimizing the absolute error of dispersion relation

To obtain optimal ESGFD coefficients, I first study characteristics of $\varepsilon(\beta)$. As an example, $\varepsilon(\beta)$ is obtained through the TEM and the LSM, respectively, shown in Fig. 2, where $M = 6$. $b = 2.17$ is used in eq. (12) together with (11) to compute ESGFD coefficients c_m. In the interval $[0, b]$, ε fluctuates around zero. In the interval $[b, \pi]$, absolute values of ε increase with an increase of β. The curve of $|\varepsilon(\beta)|$ from the LSM has several peaks, whose maximum value is $\varepsilon_{\rm P}$, ε at the point P shown in Fig. 2. At the point R, $\beta = b$, $\varepsilon_{\rm R} = |\varepsilon(b)|$. I find that $\varepsilon_{\rm P} < \varepsilon_{\rm R}$. Therefore, there exists a point Q at $\beta = B$ close to R, and $\varepsilon_{\rm Q} = \varepsilon_{\rm R}$. Because the maximum absolute error in the given interval $[0, B]$ when using B to calculate $c_{\rm m}$ is greater than that using b, I adopt b instead of B to calculate $c_{\rm m}$ but find $\varepsilon_{\max}$ in the interval $[0, B]$.

For the given maximum error $\eta = 10^{-3}, 10^{-4}, 10^{-5}$, I obtain B values for different M from the TEM and the LSM shown in Table 1 and Fig. 3, where, $\varepsilon_{\max} < \eta$ is satisfied in the interval $[0, B]$ and b, used to calculate c_m, is shown in Table 2. Table 1 and Fig. 3 suggest that the LSM provides a much wider zone than the TEM for the same η and M. For example, when $M = 7$ and $\eta = 10^{-5}$, the zone with this accuracy from the TEM is $[0, 1.24]$, but the zone from the LSM broadens about two-thirds, reaching $[0, 2.00]$.

Table 3 lists ESGFD coefficients from the LSM when $\eta = 10^{-4}$. Fig. 4 shows $\varepsilon(\beta)$ for different M from the TEM and the LSM, respectively. One can see that the LSM significantly widens the range with the given maximum error $\eta = 10^{-4}$ for the same M, compared with the TEM.

2.4 A globally optimal ESGFD scheme based on minimizing the relative error of dispersion relation

Note that minimizing the absolute error leads to large relative errors near zero wavenumber (Fig. 4), which will decrease the accuracy of wave equation modelling for wavefields with small wavenumbers. To reduce the relative error near zero wavenumber, one can minimize the relative error of dispersion relation, that is, minimize formula (10) using

$$\psi_m(\beta) = 2\beta^{-1}\left\{\sin\left[(m-0.5)\beta\right] - 2(m-0.5)\sin\left(0.5\beta\right)\right\},$$

$$g(\beta) = 1 - 2\beta^{-1}\sin\left(0.5\beta\right). \tag{17}$$

Then, c_m can be obtained by using eq. (12) together with (17) and (9).

Fig. 5 shows $\varepsilon(\beta)$ for different M by the LSM of minimizing the relative error of ESGFD dispersion relation. It can be observed that the relative errors near zero wavenumber are generally smaller than those obtained by the LSM of minimizing the absolute error in Fig. 4. Table 4 shows B values for different M from the LSM of minimizing the relative error for the given maximum error $\eta = 10^{-3}, 10^{-4}, 10^{-5}$. Table 5 displays b values used to calculate c_m. Table 6 lists ESGFD coefficients from the LSM of minimizing the relative error when $\eta = 10^{-4}$.

Table 6. Optimized ESGFD coefficients by the LSM of minimizing the relative error of dispersion relation for the maximum relative error $\eta = 10^{-4}$.

Coefficient	$M = 2$	$M = 3$	$M = 4$	$M = 5$	
c_1	0.1129042E+1	0.1185991E+1	0.1217990E+1	0.1236607E+1	
c_2	−0.4301412E-1	−0.7249965E-1	−0.9382142E-1	−0.1082265E+0	
c_3		0.6301572E-2	0.1507536E-1	0.2343440E-1	
c_4			−0.1700324E-2	−0.5033546E-2	
c_5				0.6817483E-3	
Coefficient	$M = 6$	$M = 7$	$M = 8$	$M = 9$	$M = 10$
c_1	0.1247662E+1	0.1254799E+1	0.1259312E+1	0.1262502E+1	0.1264748E+1
c_2	−0.1175538E+0	−0.1238928E+0	−0.1280347E+0	−0.1310244E+0	−0.1331606E+0
c_3	0.2997970E-1	0.3494371E-1	0.3841945E-1	0.4103928E-1	0.4296909E-1
c_4	−0.8719078E-2	−0.1208897E-1	−0.1473229E-1	−0.1686807E-1	−0.1851897E-1
c_5	0.2215897E-2	0.4132531E-2	0.5924913E-2	0.7530520E-2	0.8861071E-2
c_6	−0.3462075E-3	−0.1197110E-2	−0.2248618E-2	−0.3345071E-2	−0.4347073E-2
c_7		0.2122227E-3	0.7179226E-3	0.1380367E-2	0.2076101E-2
c_8			−0.1400855E-3	−0.4808410E-3	−0.9164925E-3
c_9				0.1023759E-3	0.3437446E-3
c_{10}					−0.7874250E-4

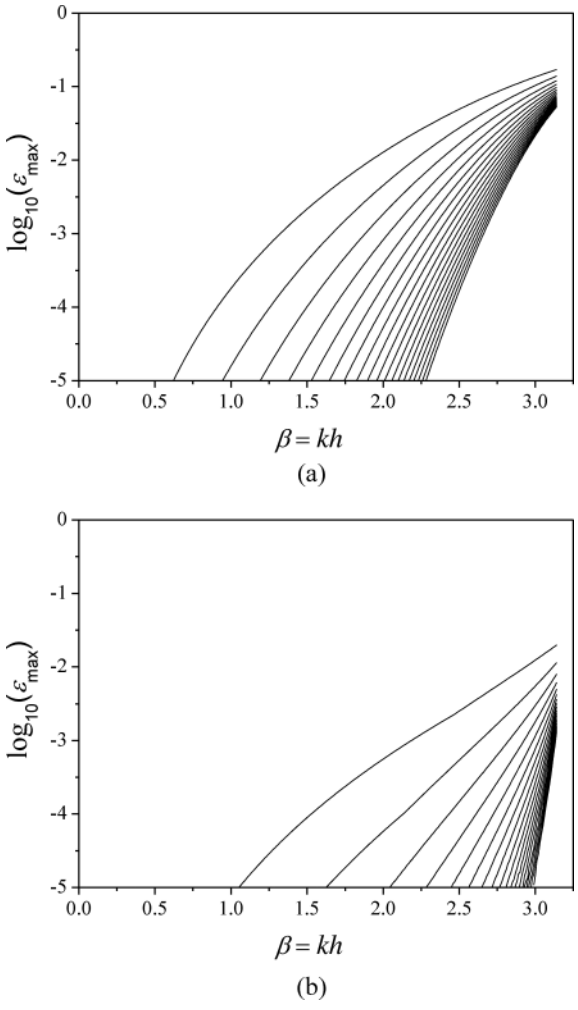

Figure 6. Variations of $\log_{10}(\varepsilon_{\max})$ of ISGFD with b for different M by the TEM (a) and the LSM (b), respectively. From top to bottom, lines are from $M = 2, 3, \ldots, 20$, respectively. Maximum values are calculated in the interval $[0, B]$.

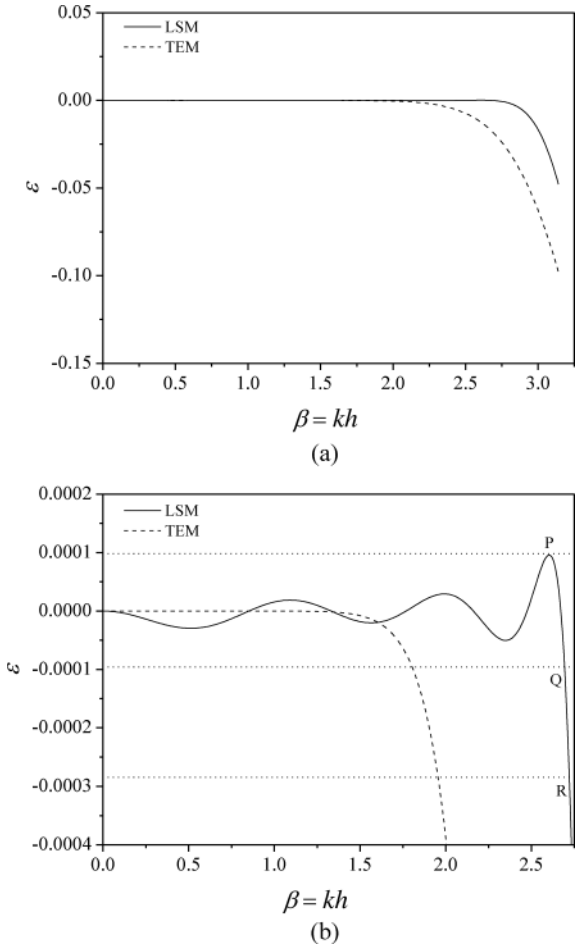

Figure 7. $\varepsilon(\beta)$ of ISGFD (a) and its zoom (b) by the TEM and the LSM, respectively. $M = 6$. For the LSM, $b = 2.72$ is used in eq. (7) together with (23) and (21) to calculate c_m and a, and their values are shown in Table 9. At the points R and Q, $\beta = b$ and $\beta = B$. At the points P and Q, $|\varepsilon|$ have the same value.

Table 7. The B values of ISGFD for different M and maximum relative errors η from the TEM and the LSM, respectively. $\varepsilon_{\max} < \eta$ is satisfied in the interval $[0, B]$.

M	B					
	$\eta = 10^{-3}$		$\eta = 10^{-4}$		$\eta = 10^{-5}$	
	TEM	LSM	TEM	LSM	TEM	LSM
2	1.32	2.12	0.90	1.49	0.62	1.03
3	1.66	2.57	1.25	2.08	0.94	1.59
4	1.88	2.77	1.49	2.39	1.19	2.01
5	2.03	2.88	1.67	2.57	1.38	2.25
6	2.14	2.94	1.80	2.69	1.52	2.41
7	2.23	2.99	1.91	2.77	1.64	2.54
8	2.30	3.01	2.00	2.82	1.74	2.62
9	2.35	3.03	2.07	2.88	1.82	2.69
10	2.40	3.05	2.13	2.91	1.89	2.74
11	2.44	3.07	2.18	2.93	1.95	2.78
12	2.48	3.08	2.23	2.96	2.00	2.81
13	2.51	3.08	2.27	2.97	2.05	2.84
14	2.54	3.09	2.30	2.99	2.09	2.87
15	2.56	3.09	2.33	3.00	2.13	2.89
16	2.58	3.10	2.36	3.01	2.17	2.91
17	2.60	3.10	2.39	3.02	2.20	2.93
18	2.62	3.10	2.41	3.02	2.23	2.94
19	2.64	3.11	2.43	3.04	2.25	2.96
20	2.65	3.11	2.45	3.05	2.28	2.97
30	2.76	3.13	2.59	3.08	2.44	3.03
40	2.78	3.13	2.61	3.10	2.47	3.09
50	2.94	3.13	2.62	3.11	2.44	3.09

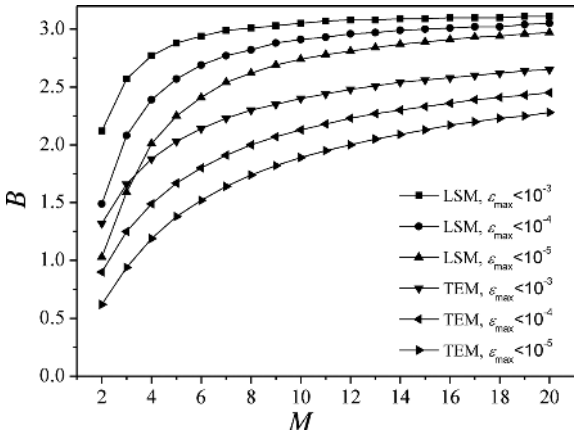

Figure 8. Variations of B of ISGFD with M for different maximum errors η by the TEM and the LSM, respectively. $\varepsilon_{\max} < \eta$ in the interval $[0, B]$.

3 OPTIMAL ISGFD SCHEME

Implicit finite differences are usually considered expensive due to necessitating solving more equations and thus are not popular.Liu & Sen (2009a) derived an implicit SGFD scheme with an arbitrary-order accuracy, which only involves solving tridiagonal matrix equations. Their efficiency analysis and numerical modelling results for elastic wave propagation demonstrate that a high-order ESGFD can be replaced by an ISGFD of some order, which will improve the accuracy without increasing the computational cost. Next, I will develop an optimal scheme for this ISGFD.

Table 8. The b values of ISGFD used to calculate ISGFD coefficients by the LSM for different M and maximum relative errors η. $\varepsilon_{\max} < \eta$ is satisfied in the interval $[0, B]$, B is shown in Table 7.

M	b		
	$\eta = 10^{-3}$	$\eta = 10^{-4}$	$\eta = 10^{-5}$
2	2.18	1.52	1.05
3	2.63	2.13	1.62
4	2.82	2.43	2.04
5	2.92	2.61	2.28
6	2.98	2.72	2.44
7	3.02	2.80	2.56
8	3.04	2.85	2.64
9	3.06	2.90	2.71
10	3.08	2.93	2.76
11	3.09	2.95	2.80
12	3.10	2.98	2.83
13	3.10	2.99	2.86
14	3.11	3.01	2.89
15	3.11	3.02	2.91
16	3.12	3.03	2.92
17	3.12	3.04	2.94
18	3.12	3.04	2.95
19	3.13	3.05	2.97
20	3.13	3.06	2.98
30	3.14	3.09	3.04
40	3.14	3.11	3.10
50	3.14	3.12	3.10

3.1 ISGFD coefficients calculated with the LS method

I use the following ISGFD formula

$$q(x-h) + aq(x) + q(x+h)$$

$$\approx \frac{1}{h}\sum_{m=1}^{M} c_m \left[p(x+mh-0.5h) - p(x-mh+0.5h)\right], \tag{18}$$

where $q(x) = \mathrm{d}p(x)/\mathrm{d}x$. It should be noted that ISGFD coefficients c_m and a here are a little different from those used by Liu & Sen (2009a, eq. 22).

Substitute eq. (2) into (18) and obtain

$$(a + 2\cos\beta)\,\beta \approx 2\sum_{m=1}^{M} c_m \sin\left[(m-0.5)\,\beta\right]. \tag{19}$$

Similarly, I introduce the following constraint condition:

$$\frac{2\sum_{m=1}^{M} c_m \sin\left[(m-0.5)\beta\right]}{a + 2\cos\beta} \to \beta \text{ while } \beta \to 0. \tag{20}$$

Then, I have

$$a = \sum_{m=1}^{M} (2m-1)\,c_m - 2. \tag{21}$$

Substitute eq. (21) into (19) and obtain

$$\sum_{m=1}^{M} \left\{\sin\left[(m-0.5)\,\beta\right] - (m-0.5)\,\beta\right\} c_m \approx (\cos\beta - 1)\,\beta. \tag{22}$$

Therefore, ISGFD coefficients can be obtained by minimizing formula (6) in which $\varphi_m(\beta)$ and $f(\beta)$ are replaced by

$$\varphi_m(\beta) = \sin\left[(m-0.5)\,\beta\right] - (m-0.5)\,\beta, \quad f(\beta) = (\cos\beta - 1)\,\beta. \tag{23}$$

Table 9. Optimized ISGFD coefficients by the LSM for the maximum relative error $\eta = 10^{-4}$.

Coefficient	$M = 2$	$M = 3$	$M = 4$	$M = 5$	
c_1	0.5881035E+1	0.3088697E+1	0.2161954E+1	0.1751338E+1	
c_2	0.6742072E+0	0.8577444E+0	0.9368543E+0	0.9761374E+0	
c_3		−0.1841475E-1	−0.3440668E-1	−0.4463936E-1	
c_4			0.2573790E-2	0.5668994E-2	
c_5				−0.6911326E-3	
a	0.5903656E+1	0.3569856E+1	0.2818500E+1	0.2490016E+1	
Coefficient	$M = 6$	$M = 7$	$M = 8$	$M = 9$	$M = 10$
c_1	0.1543395E+1	0.1420907E+1	0.1348385E+1	0.1294668E+1	0.1261059E+1
c_2	0.9971551E+0	0.1009922E+1	0.1017619E+1	0.1023384E+1	0.1027022E+1
c_3	−0.5087534E-1	−0.5489364E-1	−0.5742193E-1	−0.5935320E-1	−0.6059709E-1
c_4	0.7957645E-2	0.9634017E-2	0.1074320E-1	0.1162992E-1	0.1221332E-1
c_5	−0.1582171E-2	−0.2314457E-2	−0.2869939E-2	−0.3325840E-2	−0.3644468E-2
c_6	0.2587313E-3	0.5988390E-3	0.8694339E-3	0.1124697E-2	0.1305584E-2
c_7		−0.1213737E-3	−0.2672211E-3	−0.4003994E-3	−0.5123380E-3
c_8			0.6316408E-4	0.1420346E-3	0.2035563E-3
c_9				−0.3874797E-4	−0.7994814E-4
c_{10}					0.2420280E-4
a	0.2324794E+1	0.2227823E+1	0.2170542E+1	0.2128169E+1	0.2101687E+1

Then, c_m of the LS-based ISGFD can be obtained by solving eq. (7) together with (23). a can be obtained by eq. (21).

3.2 Accuracy analysis

I compare the LS-based ISGFD with the TE-based ISGFD, whose coefficients c_m can be obtained by solving

$$\sum_{m=1}^{M} (2m-1)^{2n+1} c_m = (2n+1)2^{2n+1}, \quad (n = 1, 2, \ldots, M). \tag{24}$$

a can be obtained by eq. (21).

To check the accuracy, I compute the rms error ε_r and the maximum error $\varepsilon_{\max}$ using eqs (14), (15) and

$$\varepsilon(\beta) = \frac{2\sum_{m=1}^{M} c_m \sin[(m-0.5)\beta]}{(a + 2\cos\beta)\,\beta} - 1. \tag{25}$$

Fig. 6 displays variations of $\log_{10}(\varepsilon_{\max})$ with b for different M by the TEM and the LSM of minimizing the error of ISGFD dispersion relation, respectively. It also demonstrates that the error increases with increasing b and decreasing M, and the LSM has a wider wavenumber range than the TEM for the same maximum error. Fig. 7 shows $\varepsilon(\beta)$ by the TEM and the LSM of minimizing the error of ISGFD dispersion relation, respectively, where $M = 6$. $b = 2.72$ is adopted in eq. (7) together with (23) to calculate FD coefficients c_m. Figs 7 and 2 have similar characteristics.

3.3 An optimal ISGFD scheme

Similarly, for the given maximum error $\eta = 10^{-3}, 10^{-4}, 10^{-5}$, I obtain B values for different M from the TEM and the LSM shown in Table 7 and Fig. 8, where $\varepsilon_{\max} < \eta$ is satisfied in the interval $[0, B]$ and b, used to calculate c_m, is shown in Table 8. Table 7 and Fig. 8 show that the LSM gives a much wider zone than the TEM for the same η and M. Table 9 gives FD coefficients from the LSM when $\eta = 10^{-4}$. Fig. 9 displays $\varepsilon(\beta)$ for different M from the TEM and the LSM. The figure shows that the LSM greatly enlarges the range with the given maximum error $\eta = 10^{-4}$ for the same M, compared to the TEM.

4 NUMERICAL EXAMPLES

I give two examples of 2-D elastic SGFD modelling for a homogeneous model and a heterogeneous model, respectively, to further demonstrate the advantages of the LS-based ESGFD method (ESGFDM) and the ISGFD method (ISGFDM). The displacement-stress relations of elastodynamic equations (e.g. Virieux 1986; Liu & Sen 2012) in isotropic elastic medium are adopted for modelling.

First, I give SGFD coefficients used in the following modelling examples. They are computed using $b = 2.9$ and $\eta = 10^{-4}$, which suggests that the absolute value of the relative dispersion error is less than 10^{-4} in the interval [0, 2.9] of β. $M = 228$ for the TE-based ESGFDM, $M = 19$ for the LS-based ESGFDM and $M = 10$ for the LS-based ISGFDM should be adopted to satisfy the accuracy requirement. Obtained ESGFD and ISGFD coefficients with $M = 19$ and $M = 10$ are shown in Tables 10 and 11, respectively.

Fig. 10 shows the dispersion error $\varepsilon(\beta)$ of the ESGFD and the ISGFD. One can see that the LS-based ESGFDM and ISGFDM significantly broaden the wavenumber range compared to the TEMs for the same operator length. In the following examples, these SGFD coefficients are used, and the mirror–image symmetry boundary condition (Chang & Liu 2013) is adopted to increase the accuracy and the stability of the implicit finite-difference method as well as the hybrid absorbing boundary condition (ABC; Liu & Sen 2012) to reduce unwanted reflections from model boundaries. The reference solution is calculated by the pseudospectral method.

The first example applies for a homogeneous model. Fig. 11 displays snapshots by the pseudospectral method, TE- and LS-based ESGFDM and ISGFDM. Differences of these snapshots are also shown. In this example, $v_p = 2000\,\mathrm{m\,s^{-1}}$, $v_s = 1000\,\mathrm{m\,s^{-1}}$, $h = 10\,\mathrm{m}$, $\tau = 1\,\mathrm{ms}$. Ricker wavelet with main frequency of 30 Hz, located in the centre of the model, is added into x-component displacement to generate vibrations. The hybrid ABC is adopted for four boundaries and the absorbing boundary layer has a thickness of 10 grids. Fig. 11 suggests that

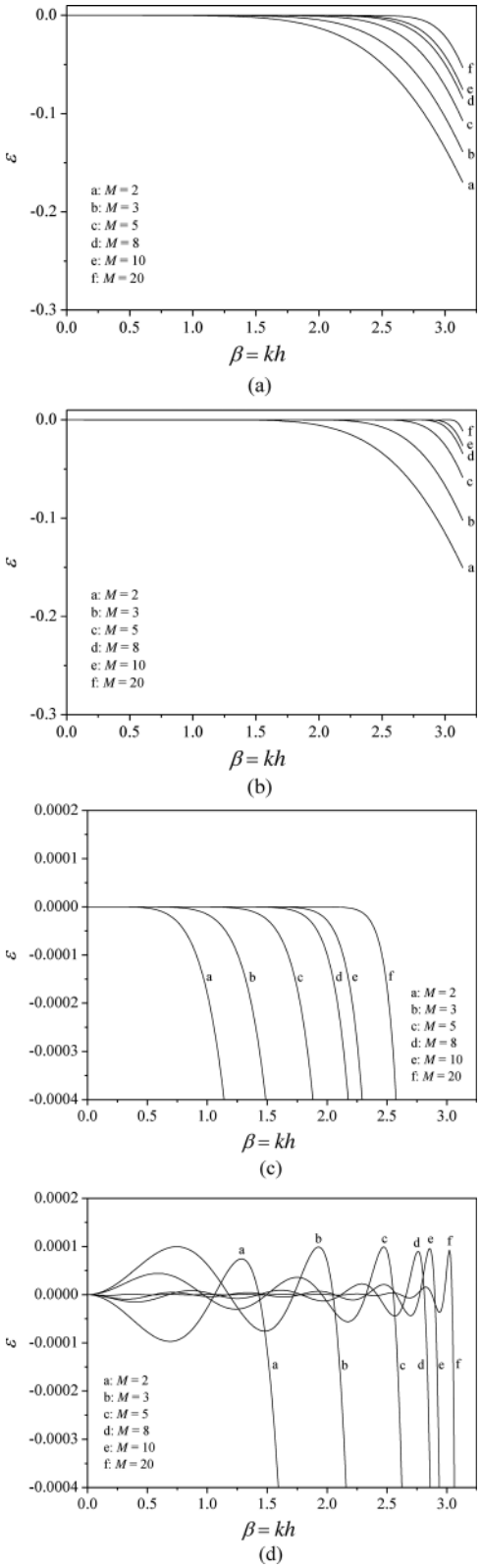

Figure 9. $\varepsilon(\beta)$ of ISGFD for different M by the TEM and the LSM, respectively. (a) is by the TEM and (b) by the LSM. (c) is zoom of (a) and (d) is zoom of (b). FD coefficients of the LSM with the maximum error $\eta = 10^{-4}$ used in the figure ($M = 2, 3, 5, 8, 10$) are listed in Table 9.

Table 10. Optimized ESGFD coefficients by the TEM and the LSM for the maximum relative error $\eta = 10^{-4}$ in the interval [0, 2.9] of β.

Coefficient	TE-based ESGFD	LS-based ESGFD
c_1	0.1256598E+1	0.1271216E+1
c_2	−0.1256598E+0	−0.1394578E+0
c_3	0.3662086E-1	0.4893614E-1
c_4	−0.1358844E-1	−0.2402039E-1
c_5	0.5360981E-2	0.1379334E-1
c_6	−0.2093441E-2	−0.8643880E-2
c_7	0.7794041E-3	0.5709894E-2
c_8	−0.2701934E-3	−0.3896436E-2
c_9	0.8570149E-4	0.2711002E-2
c_{10}	−0.2450310E-4	−0.1905154E-2
c_{11}	0.6224925E-5	0.1342289E-2
c_{12}	−0.1383840E-5	−0.9420260E-3
c_{13}	0.2644830E-6	0.6543898E-3
c_{14}	−0.4251591E-7	−0.4468455E-3
c_{15}	0.5583919E-8	0.2973663E-3
c_{16}	−0.5749006E-9	−0.1905168E-3
c_{17}	0.4348520E-10	0.1150882E-3
c_{18}	−0.2147636E-11	−0.6229052E-4
c_{19}	0.5193877E-13	0.1996929E-4

Table 11. Optimized ISGFD coefficients by the TEM and the LSM for the maximum relative error $\eta = 10^{-4}$ in the interval [0, 2.9] of β.

Coefficient	TE-based ISGFD	LS-based ISGFD
c_1	0.1953882E+1	0.1264929E+1
c_2	0.9583780E+0	0.1026604E+1
c_3	−0.4085748E-1	−0.6045529E-1
c_4	0.4940980E-2	0.1214732E-1
c_5	−0.7322610E-3	−0.3609181E-2
c_6	0.1063789E-3	0.1285709E-2
c_7	−0.1341978E-4	−0.5007292E-3
c_8	0.1323025E-5	0.1971319E-3
c_9	−0.8852494E-7	−0.7631558E-4
c_{10}	0.2972468E-8	0.2268750E-4
a	0.2653739E+1	0.2104738E+1

(1) The modelling accuracy of the LS-based ESGFDM with $M = 19$ (Fig. 11c) is much higher than the TE-based ESGFDM with $M = 19$ (Fig. 11b);

(2) The modelling accuracy of the LS-based ISGFDM with $M = 10$ (Fig. 11e) is much higher than the TE-based ISGFDM with $M = 10$ (Fig. 11d);

(3) The differences between modelling traces from the LSM and TEM and the reference solution from the pseudospectral method show that the LSMs are more accurate than the TEMs (Fig. 11f).

The other example applies for a heterogeneous model. Fig. 12 shows seismograms by the pseudospectral method, TE- and LS-based ESGFDM and ISGFDM, for the SEG/EAGE salt model, and their differences are also displayed in the figure. The model size is 6980 m × 3980 m. The grid size is 20 m × 20 m. The time step is 1 ms. The first layer of the model is ocean water. The source is located in the first layer and its coordinate is (3500 m, 20 m). Ricker wavelet with main frequency of 20 Hz is used to generate P wave. Receivers are located on the ocean bottom. The hybrid ABC is used for four boundaries and the absorbing boundary layer has a thickness of 10 grids. Comparing Figs 12(c) with (d), (h) with (i), one can observe that the LSM provides less modelling dispersion than the TEM for

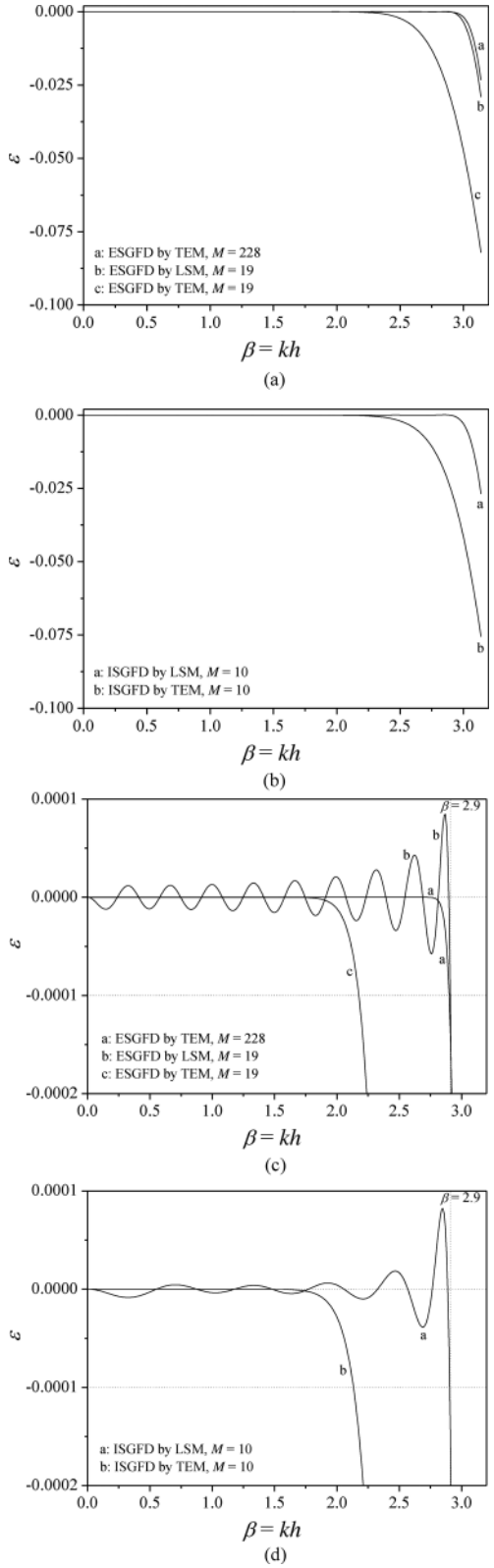

Figure 10. $\varepsilon(\beta)$ of ESGFD and ISGFD for different M by the TEM and the LSM, respectively. (a) and (b) show $\varepsilon(\beta)$ of ESGFD and ISGFD, respectively. (c) and (d) are zoom of (a) and (b), respectively. FD coefficients of the LSM are obtained using $b = 2.9$ and the maximum error $\eta = 10^{-4}$.

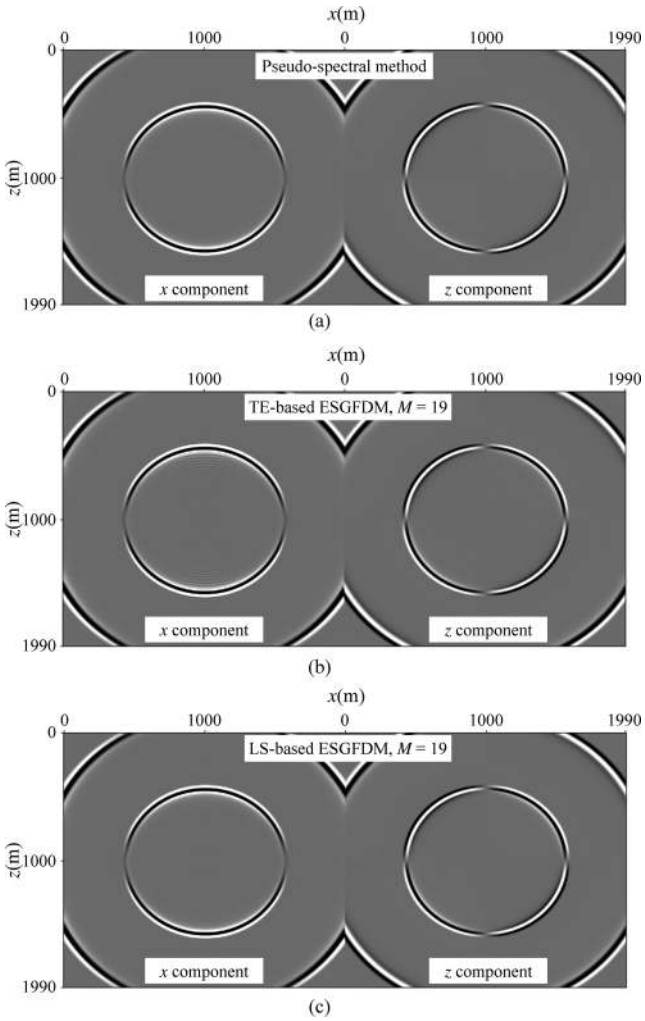

Figure 11. Snapshots at $t = 0.6$ s of elastic SGFD modelling for a homogeneous model using the pseudospectral method (a), the TE-based ESGFDM (b), the LS-based ESGFDM (c), the TE-based ISGFDM (d) and the LS-based ISGFDM (e), respectively, and their differences (f). (f) shows comparisons of x-component traces from (a) to (e); Traces 1, 2, 3, 4 and 5 with x coordinate of 1000 m are from (a), (b), (c), (d) and (e), respectively; Traces 6, 7, 8 and 9 are the differences between 2, 3, 4, 5 and 1, respectively.

the same FD operator length. The similar conclusion can be drawn by comparing Figs 12 (e) with (f), (j) with (k). Fig. 12(l) displays some traces from the pseudospectral method, TE- and LS-based ESGFDM and ISGFDM and their differences. One can also see that the LSM has a higher accuracy than the TEM.

To highlight the differences between the reference solution and the numerical solutions, I adopt the time-frequency misfit criteria (Kristeková *et al.* 2006, 2009) to evaluate them. Fig. 13 shows the globally normalized time-frequency envelope misfit between the reference solution from the pseudospectral method and numerical solutions from the SGFDM shown in Fig. 12(l). The expression for misfit calculating is taken from Kristeková *et al.* (2009; Table 1). Fig. 13 suggests that the LS-based SGFDM has a much smaller misfit than the TE-based SGFDM.

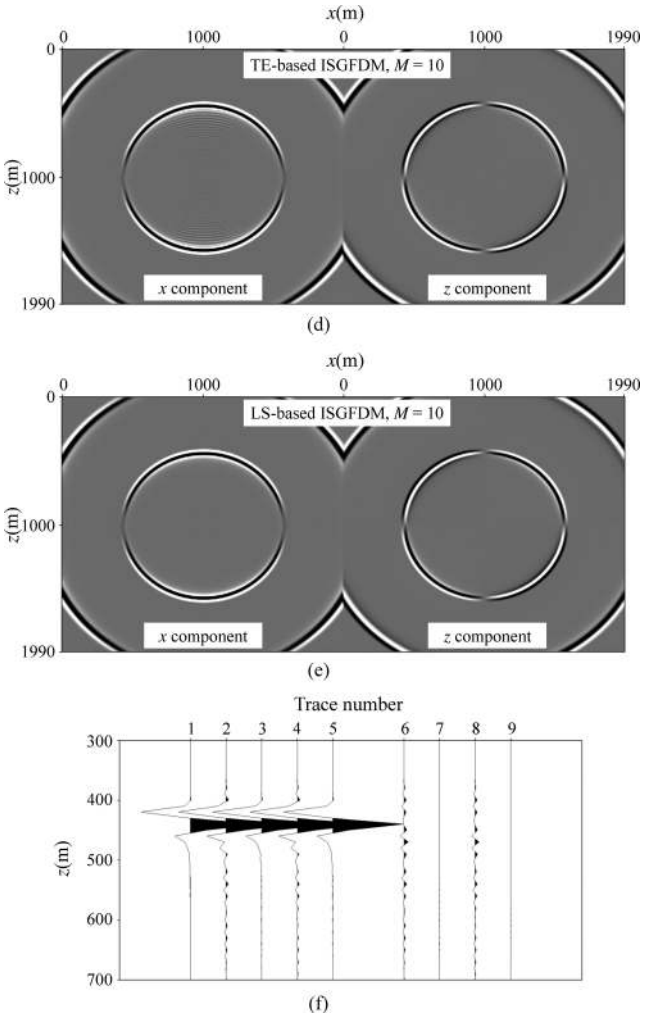

Figure 11. (*Continued*.)

For the same accuracy requirement, the LSM can adopt a shorter FD operator and thus cost less computational time than the TEM. In the second example, for 4000 time step modelling of 351 × 200 grids, CPU time on the same laptop computer is 402, 354, 361, 284 and 290 s, respectively, for the pseudospectral method, the TE-based ESGFDM with $M = 19$, the LS-based ESGFDM with $M = 19$, the TE-based ISGFDM with $M = 10$ and the LS-based ISGFDM with $M = 10$.

These two modelling examples further demonstrate the correctness and advantage of the proposed LS-based ESGFDM and ISGFDM.

5 DISCUSSION

First, I compare the stability of the TEM and the LSM. The stability condition for 2-D wave equation modelling by the $(2M)$th-order ESGFDM is

$$r \leq s, \tag{26}$$

where r is the Courant number and s is the stability factor expressed by (Liu & Sen 2011):

$$s = \frac{1}{\sqrt{2}} \left(\sum_{m=1}^{M} |c_m| \right)^{-1}. \tag{27}$$

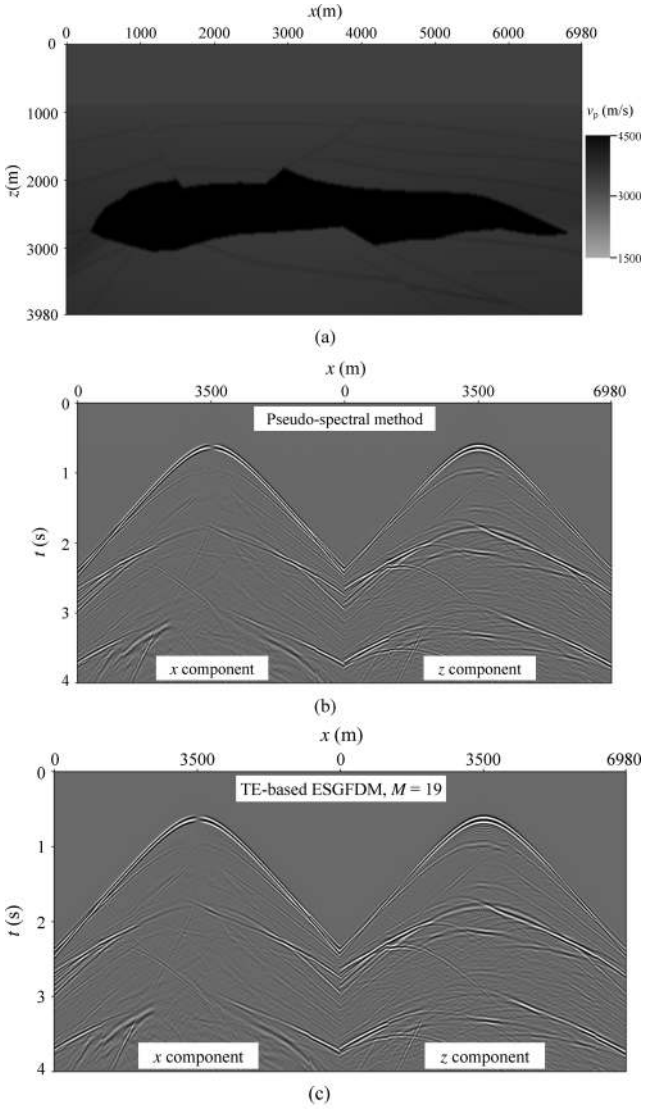

Figure 12. Seismograms of elastic SGFD modelling for a heterogeneous model using the pseudospectral method, the TE-based ESGFDM, the LS-based ESGFDM, the TE-based ISGFDM and the LS-based ISGFDM, respectively, and their differences. (a) The SEG/EAGE salt model (*S*-wave velocity and density, having the similar characteristics to *P*-wave velocity, are not shown). (b) Seismograms by the pseudospectral method. (c) Seismograms by the TE-based ESGFDM, $M = 19$. (d) Seismograms by the LS-based ESGFDM, $M = 19$. (e) Seismograms by the TE-based ISGFDM, $M = 10$. (f) Seismograms by the LS-based ISGFDM, $M = 10$. (g) Zoom of (b). (h) Zoom of (c). (i) Zoom of (d). (j) Zoom of (e). (k) Zoom of (f). (l) Some traces from (g), (h), (i), (j), (k) and their differences; Traces 1, 2, 3, 4, 5 with x coordinate of 5400 m are from (g), (h), (i), (j), (k), respectively; Traces 6, 7, 8, 9 are the differences between 2, 3, 4, 5 and 1, respectively.

Fig. 14 shows the variation of the stability factor s by the TEM and the LSM for the given error $\eta = 10^{-4}$. It can be seen that the area of r for stable recursion reduces with the increase of M, and the stability condition of the LSM is slightly stricter than that of the TEM.

Finally, I briefly compare my method with that of Tam & Webb (1993) who studied optimal spatial FD coefficients for the first-order derivative on standard grids. It should be noted that they

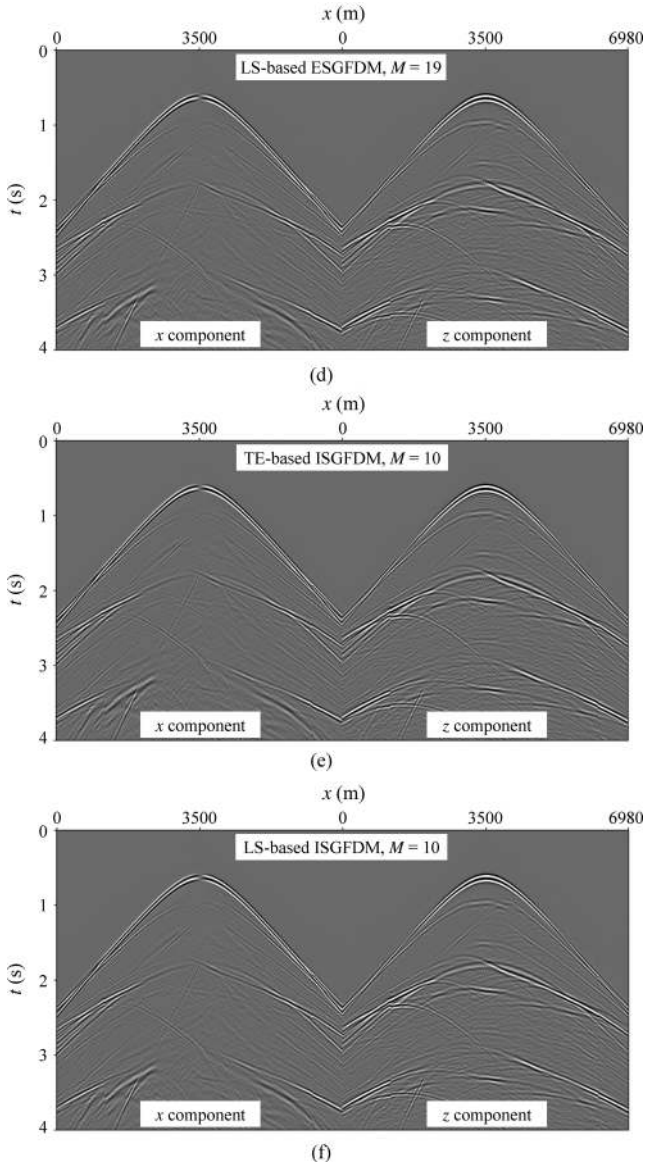

Figure 12. (*Continued*.)

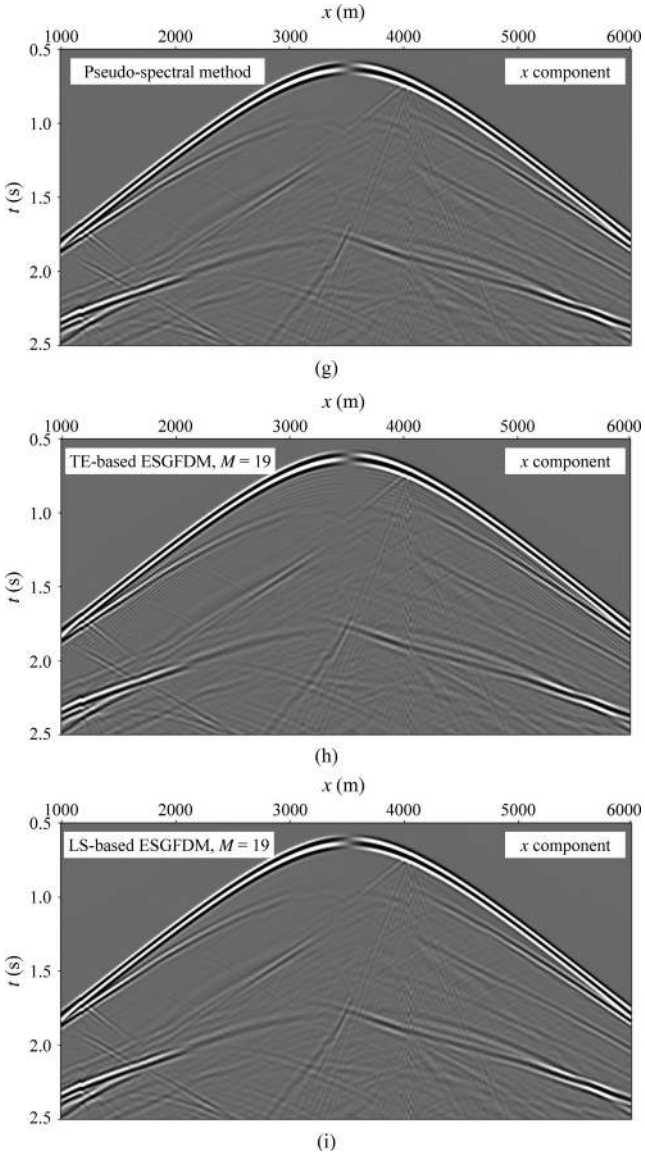

Figure 12. (*Continued*.)

calculated the FD coefficients by minimizing the square error over a fixed interval $[-0.5\pi, 0.5\pi]$ and thus the FD coefficients are only dependent on the operator length. Their method is suitable for broad-band modelling. I studied optimal explicit and implicit spatial FD coefficients for the first-order derivative on staggered grids. The optimal FD coefficients are dependent on the chosen error over the given wavenumber range. My method is appropriate for band-limited modelling. When the given wavenumber range equals $[-0.5\pi, 0.5\pi]$, my method is also suitable for broad-band modelling.

6 CONCLUSIONS

I have developed new LS-based schemes to obtain explicit and implicit FD coefficients on staggered grids when the wavenumber range $[0, b]$ and the maximum error η are given. Compared to the SGFD method based on Taylor-series expansion, the schemes based on LS can adopt the shorter operator length to achieve the same accuracy, greatly reducing the computational cost. Dispersion analyses and numerical modelling show the advantages of the proposed schemes. They can also be used in partly rotated staggered-grid modelling.

ACKNOWLEDGEMENTS

I thank the Editor, Dr. Andrea Morelli, and two anonymous reviewers for their valuable comments. This research is supported by National Nature Science Foundation of China (NSFC) under contract number 41074100, Program for New Century Excellent Talents in University of Ministry of Education of China under contract number NCET-10–0812, the National High Technology Research and Development Program of China (863 program) under contract number 2013AA064201 and the Scientific Research Foundation for the Returned Overseas Chinese Scholars, State Education Ministry.

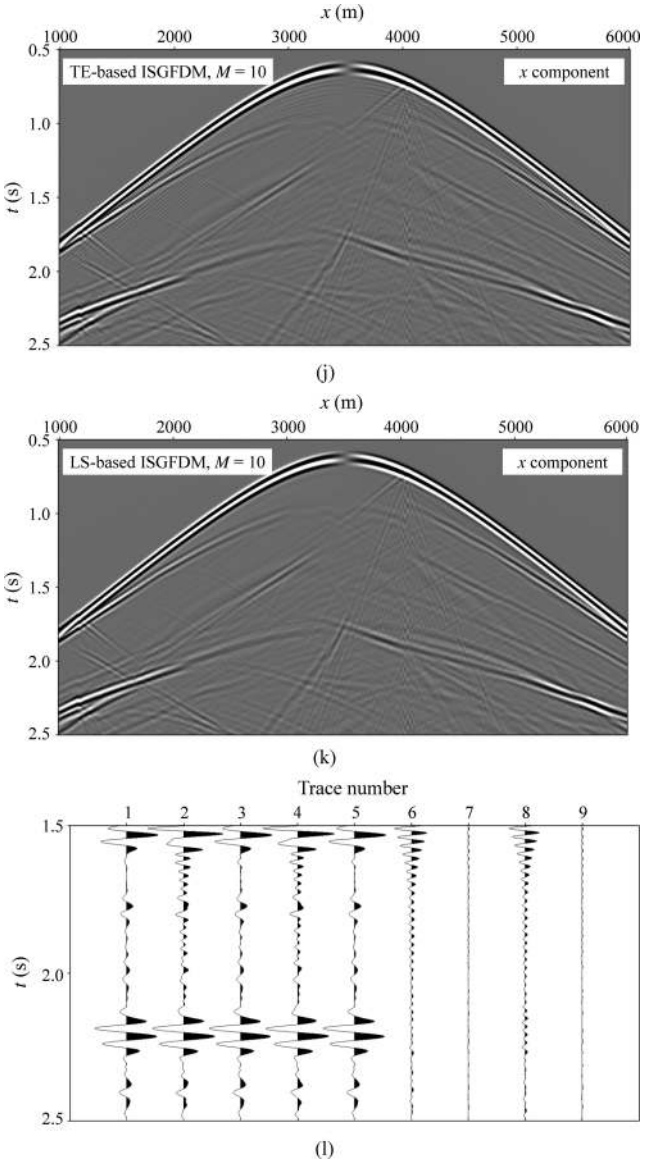

Figure 12. (*Continued*.)

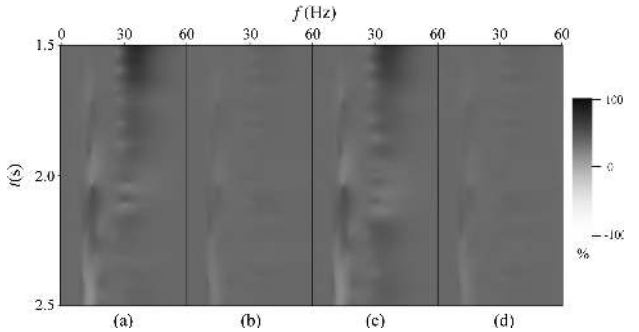

Figure 13. Globally normalized time-frequency envelope misfit between the reference solution from the pseudospectral method and numerical solutions from the SGFD methods shown in Fig. 12(l). (a) Between Trace 2 by the TE-based ESGFDM and 1 by the pseudospectral method. (b) Between Trace 3 by the LS-based ESGFDM and 1. (c) Between Trace 4 by the TE-based ISGFDM and 1. (d) Between Trace 5 by the LS-based ISGFDM and 1.

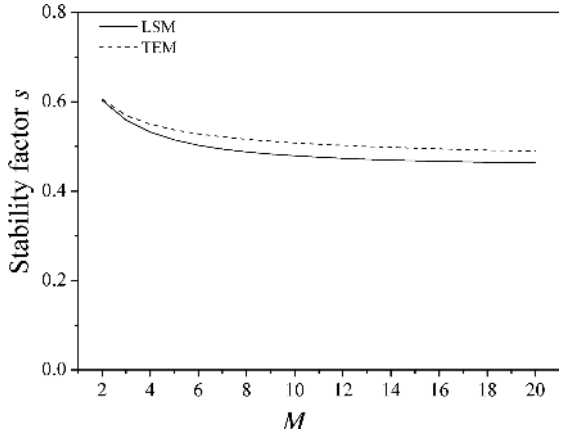

Figure 14. The variation of the stability factor s with M for 2-D wave equation modelling by the (2M)th-order ESGFDM.

REFERENCES

Bansal, R. & Sen, M.K., 2008. Finite-difference modelling of S-wave splitting in anisotropic media, *Geophys. Prospect.,* **56,** 293–312.

Bohlen, T., 2002. Parallel 3-D viscoelastic finite-difference seismic modeling, *Comput. Geosci.,* **28,** 887–899.

Chang, S. & Liu, Y., 2013. A truncated implicit high-order finite-difference scheme combined with boundary conditions, *Appl. Geophys.,* **10,** 53–62.

Chen, J., 2012. An average-derivative optimal scheme for frequency-domain scalar wave equation, *Geophysics,* **77,** T201–T210.

Chu, C. & Stoffa, P.L., 2012a. Implicit finite-difference simulations of seismic wave propagation, *Geophysics,* **77,** T57–T67.

Chu, C. & Stoffa, P.L., 2012b. Determination of finite-difference weights using scaled binomial windows, *Geophysics,* **77,** W17–W26.

Crase, E., 1990. High-order (space and time) finite-difference modeling of the elastic wave equation, *SEG Expanded Abst.,* **9,** 987–991.

Di Bartolo, L., Dors, C. & Mansur, W.J., 2012. A new family of finite-difference schemes to solve the heterogeneous acoustic wave equation, *Geophysics,* **77,** T187–T199.

Dong, L., Ma, Z., Cao, J., Wang, H., Geng, J., Lei, B. & Xu, S., 2000. A staggered-grid high-order difference method of one-order elastic wave equation, *Chinese J. Geophys.-Chinese Ed.,* **43,** 411–419.

Du, Q., Li, B. & Hou, B., 2009. Numerical modeling of seismic wavefields in transversely isotropic media with a compact staggered-grid finite difference scheme, *Appl. Geophys.,* **6,** 42–49.

Etgen, J.T. & O'Brien, M.J., 2007. Computational methods for large-scale 3D acoustic finite-difference modeling: a tutorial, *Geophysics,* **72,** SM223–SM230.

Fornberg, B., 1987. The pseudospectral method—comparisons with finite differences for the elastic wave equation, *Geophysics,* **52,** 483–501.

Fornberg, B., 1998. Calculation of weights in finite difference formulas, *SIAM Rev.,* **40,** 685–691.

Gottschämer, E. & Olsen, K., 2001. Accuracy of the explicit planar free surface boundary condition implemented in a fourth-order staggered-grid velocity-stress finite-difference scheme, *Bull. seism. Soc. Am.,* **91,** 617–623.

Graves, R.W., 1996. Simulating seismic wave propagation in 3D elastic media using staggered-grid finite differences, *Bull. seism. Soc. Am.,* **86,** 1091–1106.

Hayashi, K., Burns, D.R. & Toksöz, M.N., 2001. Discontinuous-grid finite-difference seismic modeling including surface topography, *Bull. seism. Soc. Am.,* **91,** 1750–1764.

Hestholm, S., 2003. Elastic wave modeling with free surfaces: stability of long simulations, *Geophysics,* **68,** 314–321.

Hestholm, S., 2009. Acoustic VTI modeling using high-order finite differences, *Geophysics,* **74,** T67–T73.

Hestholm, S. & Ruud, B., 1998. 3-D finite-difference elastic wave modeling including surface topography, *Geophysics,* **63,** 613–622.

Holberg, O., 1987. Computational aspects of the choice of operator and sampling interval for numerical differentiation in large-scale simulation of wave phenomena, *Geophys. Prospect.,* **35,** 629–655.

Igel, H., Mora, P. & Riollet, B., 1995. Anisotropic wave propagation through finite-difference grids, *Geophysics,* **60,** 1203–1216.

JafarGandomi, A. & Takenaka, H., 2009. Non-standard FDTD for elastic wave simulation: two-dimensional P-SV case, *Geophys. J. Int.,* **178,** 282–302.

Jastram, C. & Behle, A., 1993. Accurate finite-difference operators for modelling the elastic wave equation, *Geophys. Prospect.,* **41,** 453–458.

Kindelan, M., Kamel, A. & Sguazzero, P., 1990. On the construction and efficiency of staggered numerical differentiators for the wave equation, *Geophysics,* **55,** 107–110.

Kosloff, D., Pestana, R.C. & Tal-Ezer, H., 2010. Acoustic and elastic numerical wave simulations by recursive spatial derivative operators, *Geophysics,* **75,** T167–T174.

Kristek, J., Moczo, P. & Archuleta, R.J., 2002. Efficient methods to simulate planar free surface in the 3D 4th-order staggered-grid finite-difference schemes, *Stud. Geophys. Geod.,* **6,** 355–381.

Kristeková, M., Kristek, J., Moczo, P. & Day, S.M., 2006. Misfit criteria for quantitative comparison of seismograms, *Bull. seism. Soc. Am.,* **96,** 1836–1850.

Kristeková, M., Kristek, J. & Moczo, P., 2009. Time-frequency misfit and goodness-of-fit criteria for quantitative comparison of time signals, *Geophys. J. Int.,* **178,** 813–825.

Krüger, O.S., Saenger, E.H. & Shapiro, S., 2005. Scattering and diffraction by a single crack: an accuracy analysis of the rotated staggered grid, *Geophys. J. Int.,* **162,** 25–31.

Lan, H. & Zhang, Z., 2011. Three-dimensional wave-field simulation in heterogeneous transversely isotropic medium with irregular free surface, *Bull. seism. Soc. Am.,* **101,** 1354–1370.

Lele, S.K., 1992. Compact finite difference schemes with spectral-like resolution, *J. Comput. Phys.,* **103,** 16–42.

Levander, A.R., 1988. Fourth-order finite-difference P-SV seismograms, *Geophysics,* **53,** 1425–1436.

Liu, Y., 2013. Globally optimal finite-difference schemes based on least squares, *Geophysics,* **78,** T113–T132.

Liu, Y. & Sen, M.K., 2009a. An implicit staggered-grid finite-difference method for seismic modeling, *Geophys. J. Int.,* **179,** 459–474.

Liu, Y. & Sen, M.K., 2009b. Numerical modeling of wave equation by truncated high-order finite difference method, *Earthq. Sci.,* **22,** 205–213.

Liu, Y. & Sen, M.K., 2011. Scalar wave equation modeling with time-space domain dispersion-relation-based staggered-grid finite-difference schemes, *Bull. seism. Soc. Am.,* **101**,141–159.

Liu, Y. & Sen, M.K., 2012. A hybrid absorbing boundary condition for elastic staggered-grid modeling, *Geophys. Prospect.,* **60,** 1114–1132.

Liu, Y., Li, C. & Mou, Y., 1998. Finite-difference numerical modeling of any even-order accuracy, *Oil Geophys. Prospect.,* **33,** 1–10.

Lombard, B., Piraux, J., Gélis, C. & Virieux, J., 2008. Free and smooth boundaries in 2D FD schemes transient elastic waves, *Geophys. J. Int.,* **172,** 252–261.

Madariaga, R., 1976. Dynamics of an expanding circular fault, *Bull. seism. Soc. Am.,* **66,** 639–666.

Mittet, R., 2002. Free-surface boundary conditions for elastic staggered-grid modeling schemes, *Geophysics,* **67,** 1616–1623.

Moczo, P., Kristek, J. & Halada, L., 2000. 3D fourth-order staggered-grid finite-difference schemes: stability and grid dispersion, *Bull. seism. Soc. Am.,* **90,** 587–603.

Moczo, P., Kristek, J., Vavrycuk, V., Archuleta, R. & Halada, L., 2002. Heterogeneous staggered-grid finite-difference modeling of seismic motion with volume harmonic and arithmetic averaging of elastic moduli and densities, *Bull. seism. Soc. Am.,* **92,** 3042–3066.

Ohminato, T. & Chouet, B.A., 1997. A free-surface boundary condition for including 3D topography in the finite-difference method, *Bull. seism. Soc. Am.,* **87,** 494–515.

Operto, S., Virieux, J., Amestoy, P., L'Excellent, J.Y., Giraud, L. & Ali, H.B.H., 2007. 3D finite-difference frequency-domain modeling of visco-acoustic wave propagation using a massively parallel direct solver: a feasibility study, *Geophysics,* **72,** SM195–SM211.

Pei, Z., Fu, L., Sun, W., Jiang, T. & Zhou, B., 2012. Anisotropic finite-difference algorithm for modeling elastic wave propagation in fractured coalbeds, *Geophysics,* **77,** C13–C26.

Robertsson, J.O.A., 1996. A numerical free-surface condition for elastic/viscoelastic finite-difference modeling in the presence of topography, *Geophysics,* **61,** 1921–1934.

Robertsson, J.O.A., Blanch, J.O. & Symes, W.W., 1994a. Viscoelastic finite-difference modeling, *Geophysics,* **59,** 1444–1456.

Robertsson, J.O.A., Blanch, J.O., Symes, W.W. & Burrus, C.S., 1994b. Galerkin-wavelet modeling of wave propagation: optimal finite difference stencil design, *Math. Comput. Model.,* **19,** 31–38.

Saenger, E.H. & Bohlen, T., 2004. Finite-difference modeling of viscoelastic and anisotropic wave propagation using the rotated staggered grid, *Geophysics,* **69,** 583–591.

Saenger, E.H. & Shapiro, S.A., 2002. Effective velocities in fractured media: a numerical study using the rotated staggered finite difference grid, *Geophys. Prospect.,* **50,** 183–194.

Saenger, E.H., Gold, N. & Shapiro, S.A., 2000. Modeling the propagation of elastic waves using a modified finite-difference grid, *Wave Motion,* **31,** 77–92.

Shan, G., 2009. Optimized implicit finite-difference and Fourier finite-difference migration for VTI media, *Geophysics,* **74,** WCA189–WCA197.

Song, X. & Fomel, S., 2011. Fourier finite-difference wave propagation, *Geophysics,* **76,** T123–T129.

Takeuchi, N. & Geller, R.J., 2000. Optimally accurate second order time-domain finite difference scheme for computing synthetic seismograms in 2-D and 3-D media, *Phys. Earth planet. Int.,* **119,** 99–131.

Tam, C.K.W. & Webb, J.C., 1993. Dispersion-relation-preserving finite difference schemes for computational acoustics, *J. Comput. Phys.,* **107,** 262–281.

Tarrass, I., Giraud, L. & Thore, P., 2011. New curvilinear scheme for elastic wave propagation in presence of curved topography, *Geophys. Prospect.,* **59,** 889–906.

Virieux, J., 1984. SH-wave propagation in heterogeneous media: velocity-stress finite-difference method, *Geophysics,* **49,** 1933–1957.

Virieux, J., 1986. P-SV wave propagation in heterogeneous media: velocity stress finite difference method, *Geophysics,* **51,** 889–901.

Yan, H. & Liu, Y., 2012. Rotated staggered grid high-order finite-difference numerical modeling for wave propagation in viscoelastic TTI media, *Chinese J. Geophys.-Chinese Ed.,* **55,** 1354–1365.

Yang, B. & Balanis, C.A., 2006. Least square method to optimize the coefficients of complex finite-difference space stencils, *IEEE Antenn. Wirel. Pr.,* **5,** 450–453.

Zhang, J., 1997. Quadrangle-grid velocity-stress finite-difference method for elastic-wave-propagation simulation, *Geophys. J. Int.,* **131,** 127–134.

Zhang, J. & Yao, Z., 2012. Globally optimized finite-difference extrapolator for strongly VTI media, *Geophysics,* **77,** T125–T135.

Zhang, J. & Yao, Z., 2013. Optimized finite-difference operator for broadband seismic wave modeling, *Geophysics,* **78,** A13–A18.

Zhang, W. & Chen, X., 2006. Traction image method for irregular free surface boundaries in finite difference seismic wave simulation, *Geophys. J. Int.,* **167,** 337–353.

Zhang, W., Zhang, Z. & Chen, X., 2012. Three-dimensional elastic wave numerical modelling in the presence of surface topography by a collocated-grid finite-difference method on curvilinear grids, *Geophys. J. Int.,* **190,** 358–378.

Zhou, B. & Greenhalgh, S.A., 1992. Seismic scalar wave equation modeling by a convolutional differentiator, *Bull. seism. Soc. Am.,* **82,** 289–303.

Zhou, H. & Zhang, G., 2011. Prefactored optimized compact finite-difference schemes for second spatial derivatives, *Geophysics,* **76,** WB87–WB95.